Data-Driven Excimer LiDAR Framework for Joint Surface Reflectivity Mapping and Atmospheric Pollutant Profiling

Sandugash Dospanbetova[1]*, Gulzat Ziyatbekova[2]*, Murat Baktybayev[3],
Botakoz Smagul[4], Yermakhan Zhabayev[5], Zhanar Bidakhmet[6]
Kazakh National Research Technical University named after K.I.Satpayev, Almaty, Kazakhstan [1, 3]
Almaty Technological University, Almaty, Republic of Kazakhstan[2]
Al-Farabi Kazakh National University, Almaty, Kazakshtan[2]
Abay Kazakh National Pedagogical University, Almaty, Kazakhstan[4, 5]
Almaty University of Power Engineering and Communications named after Gumarbek Daukeev[6]

***Abstract*—This study proposes a data-driven excimer LiDAR framework for joint surface reflectivity mapping and atmospheric pollutant profiling, integrating physics-based sensing with deep learning-based multi-source data fusion. The system utilizes ultraviolet excimer LiDAR measurements in combination with auxiliary data from UAV platforms, satellite observations, and ground-based sensors to construct a unified environmental monitoring pipeline. A structured signal processing approach is applied to extract physically meaningful features, including backscatter and extinction coefficients, as well as differential absorption parameters. These features are subsequently fused using a deep learning architecture designed to model complex nonlinear relationships across heterogeneous data sources. Experimental results demonstrate that the proposed method achieves high predictive accuracy, with improved correlation and reduced error compared to traditional LiDAR and baseline fusion approaches. The framework effectively captures both vertical atmospheric pollutant distributions and horizontal surface reflectivity patterns, enabling comprehensive environmental analysis. Validation against external datasets confirms the robustness and generalization capability of the model under varying conditions. The integration of data-driven modeling with excimer LiDAR sensing enhances system performance while maintaining real-time capability. Overall, the proposed approach provides a scalable and efficient solution for advanced environmental monitoring, contributing to the development of intelligent remote sensing systems for air quality assessment and land-cover analysis.**

Keywords*—LiDAR; data-driven modeling; multi-source data fusion; deep learning; remote sensing

I. Introduction

Monitoring the Earth's surface and atmospheric composition has become an increasingly critical task in the context of rapid urbanization, industrial expansion, and climate variability. Advanced remote sensing technologies are required to provide high-resolution, reliable, and continuous observations across spatial and temporal scales. Among these technologies, lidar has emerged as a powerful active sensing modality capable of capturing three-dimensional information about both terrestrial and atmospheric phenomena with high precision [1]. Unlike passive sensing approaches, lidar systems operate independently of solar illumination, enabling consistent data acquisition under diverse environmental conditions, including low-light and nighttime scenarios [2]. This capability makes lidar particularly suitable for applications involving environmental monitoring, air quality assessment, and geospatial analysis, where accuracy and temporal consistency are essential.

Despite these advantages, conventional lidar systems often rely on laser sources such as dye lasers, which present limitations in terms of operational complexity, wavelength flexibility, and maintenance requirements [3]. These constraints restrict their scalability for long-term monitoring and real-time deployment in dynamic environments. In contrast, excimer lasers, operating in the ultraviolet spectral region, offer distinct benefits due to their high pulse energy, short wavelength, and strong interaction with atmospheric constituents [4-6]. The ultraviolet emission enhances sensitivity to molecular absorption and scattering processes, thereby improving the detection of trace gases and fine particulate matter. Moreover, the ability of excimer-based systems to directly generate ultraviolet radiation without complex frequency conversion mechanisms simplifies system design and enhances operational robustness [7].

Recent developments in data-driven methodologies have further expanded the capabilities of lidar systems by enabling intelligent processing and interpretation of large-scale sensing data [8]. The integration of computational models with lidar measurements facilitates advanced signal analysis, noise reduction, and feature extraction, thereby improving the accuracy of retrieved environmental parameters [9]. In particular, data-driven frameworks allow for the joint analysis of surface reflectivity and atmospheric pollutant profiles, bridging the gap between terrestrial and atmospheric observations [10]. This unified perspective is essential for understanding complex environmental interactions, such as the coupling between land surface properties and pollutant dispersion dynamics [11]. Furthermore, the incorporation of multi-source data, including UAV-based sensors and satellite observations, enhances the validation and scalability of lidar-based monitoring systems.

*Corresponding author.

In this context, the present study proposes a data-driven excimer lidar framework for joint surface reflectivity mapping and atmospheric pollutant profiling. The proposed approach leverages the spectral advantages of ultraviolet lidar sensing and integrates advanced data processing strategies to achieve high-resolution environmental characterization. By combining differential absorption principles with data-driven modeling, the framework enables accurate retrieval of both surface and atmospheric parameters within a unified system architecture [12]. The study further explores system validation through multi-platform observations, demonstrating strong agreement with independent measurement sources and highlighting the robustness of the proposed methodology. This work aims to contribute to the development of next-generation intelligent sensing systems capable of supporting comprehensive environmental monitoring and decision-making processes.

II. Related Works

The evolution of lidar-based remote sensing systems has been extensively investigated in the context of atmospheric profiling and surface monitoring. Classical lidar formulations are grounded in the interaction between emitted laser pulses and atmospheric constituents, where backscatter and extinction coefficients govern signal behavior and retrieval accuracy [13]. These principles have enabled the development of high-resolution vertical profiling techniques capable of capturing aerosol distributions, cloud structures, and trace gas concentrations [14]. Furthermore, advancements in scattering theory have refined the interpretation of Rayleigh and Mie interactions, allowing improved discrimination between molecular and particulate contributions in lidar returns [15]. Such theoretical developments have laid the foundation for modern lidar systems employed in environmental and geophysical studies.

A significant advancement in lidar technology is the adoption of differential absorption lidar (DIAL), which enhances selectivity in detecting specific atmospheric species [16]. By employing wavelength pairs with distinct absorption characteristics, DIAL systems can estimate gas concentrations with high precision [17]. This methodology has been widely applied for monitoring ozone, nitrogen dioxide, and other pollutants, demonstrating its effectiveness in both ground-based and airborne platforms [18]. Additionally, multi-wavelength lidar configurations have been introduced to improve retrieval accuracy and to enable simultaneous detection of multiple atmospheric components [19]. However, these systems often require complex optical setups and precise wavelength tuning, which can limit their operational flexibility and increase system cost.

The choice of laser source remains a critical factor influencing lidar performance. Traditional systems predominantly utilize solid-state or dye lasers due to their stability and tunability [20]. Nevertheless, these sources are associated with drawbacks such as complex harmonic generation processes and maintenance-intensive operation [21]. Recent studies have explored alternative laser technologies, including excimer and ultrafast laser systems, which offer direct ultraviolet emission and enhanced interaction with atmospheric molecules [22]. Ultraviolet wavelengths exhibit strong absorption characteristics, enabling improved sensitivity in detecting trace gases and fine aerosols [23]. Moreover, advances in laser engineering have led to compact and high-power sources, facilitating the deployment of lidar systems in mobile and field-based applications [24].

In parallel with hardware advancements, data-driven approaches have emerged as a transformative direction in lidar research [25]. The integration of signal processing techniques, statistical modeling, and machine learning algorithms has significantly improved the extraction of meaningful information from noisy LiDAR data [26]. Techniques such as inversion algorithms, adaptive filtering, and probabilistic modeling have enhanced the estimation of atmospheric parameters under varying environmental conditions [27]. Furthermore, the fusion of lidar data with complementary sources, including satellite observations and UAV-based measurements, has been shown to improve spatial coverage and validation accuracy [28]. This multi-source integration framework supports more robust environmental monitoring and enables cross-platform consistency in large-scale sensing applications [29].

Recent works have also emphasized the importance of system-level optimization and error analysis in lidar-based monitoring frameworks [30]. Sources of systematic and statistical errors, including timing inaccuracies, detector noise, and atmospheric variability, have been extensively analyzed to improve measurement reliability [31]. Comparative studies have highlighted trade-offs between different lidar configurations, particularly in terms of range, sensitivity, and computational complexity [32]. Additionally, the development of real-time processing pipelines and high-speed data acquisition systems has enabled near real-time environmental assessment [33]. These advancements are particularly relevant for applications requiring rapid response, such as air quality monitoring and disaster management [34].

Despite these developments, challenges remain in achieving unified frameworks that simultaneously address surface reflectivity mapping and atmospheric pollutant profiling [35]. Existing studies often treat these tasks independently, leading to fragmented analysis and limited understanding of surface–atmosphere interactions [36]. Moreover, the scalability of lidar systems is constrained by hardware limitations and computational demands associated with large-scale data processing [37]. Emerging research has begun to address these issues through integrated architectures and hybrid sensing strategies, combining optical sensing with advanced computational models [38]. The adoption of data-driven methodologies has further facilitated the development of adaptive and intelligent lidar systems capable of handling complex environmental dynamics [39]. A comparative overview of representative lidar approaches, including their sensing capabilities, laser types, and data processing strategies, is presented in Table I, highlighting the strengths and limitations of existing methods and motivating the need for a unified data-driven excimer lidar framework.

TABLE I. COMPARATIVE ANALYSIS OF LIDAR-BASED ENVIRONMENTAL MONITORING APPROACHES

Study Type	Wavelength Range	Technique	Surface Mapping	Pollutant Detection	Data Processing	Platform	Detection Range	Accuracy (%)	Real-Time Capability
Classical Lidar [14]	IR/Visible	Backscatter	Yes	Limited	Basic DSP	Ground	High	85	No
Raman Lidar [15]	Visible	Raman Scattering	No	Yes	Statistical	Ground	Medium	88	No
DIAL System [16]	Tunable	Differential Absorption	Partial	Yes	Analytical	Ground/Airborne	High	90	Partial
Multi-wavelength Lidar [19]	Multi-band	Multi-spectral	Yes	Yes	Advanced DSP	Ground	High	91	Partial
UV Lidar [20]	UV	Backscatter + Absorption	Yes	Yes	Filtering	Ground	Medium	89	Partial
Satellite Lidar [21]	Multi-band	Passive-Active Hybrid	Yes	Yes	Big Data Analytics	Satellite	Very High	87	No
UAV-based Lidar [23]	Visible/UV	Backscatter	Yes	Limited	Lightweight DSP	UAV	Low	86	Yes
Hybrid Lidar System [27]	Multi-band	Combined Techniques	Yes	Yes	Fusion Models	Ground/Airborne	High	92	Partial
AI-enhanced Lidar [28]	Multi-band	Learning-based	Yes	Yes	Machine Learning	Ground	Medium	93	Yes
Fiber Laser Lidar [29]	IR	Backscatter	Yes	Limited	DSP	Ground	High	84	Yes
Ultrafast Laser Lidar [32]	UV/Visible	High-resolution	Yes	Yes	Advanced Modeling	Lab/Ground	Medium	94	No
Proposed Direction	UV	Data-driven DIAL	Yes	Yes	AI + Fusion	Multi-platform	High	>94 (expected)	Yes

III. MATERIALS AND METHODS

This section presents the methodological framework developed to enable joint surface reflectivity mapping and atmospheric pollutant profiling using a data-driven excimer LiDAR system. The approach integrates physics-based sensing principles with advanced computational modeling to ensure both accuracy and robustness in environmental monitoring. Initially, a multi-source data acquisition strategy is established, combining ultraviolet LiDAR measurements with complementary inputs from UAV platforms, satellite observations, and ground-based stations to capture heterogeneous environmental information. Subsequently, a structured signal processing pipeline is applied to transform raw LiDAR returns into reliable and physically interpretable features, including backscatter and extinction coefficients as well as differential absorption parameters [40]. These features are then incorporated into a deep learning-based data fusion model designed to learn complex relationships across modalities and to produce unified predictions for both surface and atmospheric variables. The overall methodology emphasizes synchronization, noise reduction, and feature consistency, ensuring that the integrated system can operate effectively under diverse environmental conditions while maintaining high predictive performance.

A. System Architecture and Multi-Source Data Acquisition

The proposed framework integrates heterogeneous sensing modalities into a unified acquisition pipeline, as illustrated in Fig. 1. The primary sensing unit is an excimer-laser-based LiDAR system operating at ultraviolet wavelengths (193–308 nm), enabling strong interaction with atmospheric molecules and surface materials. The received backscattered signal $P(r)$ at range r is modeled using the standard lidar equation:

$$P(r) = \frac{C\,\beta(r)}{r^2}\exp\left(-2\int_0^r \alpha(s)\,ds\right) \quad (1)$$

where, C is the system constant, $\beta(r)$ is the backscatter coefficient, and $\alpha(r)$ is the extinction coefficient.

In parallel, auxiliary data streams are acquired from UAV-based sensors (gas concentration, meteorological parameters) [41], satellite platforms (reflectance, aerosol optical depth) [42], and ground-based stations (in-situ pollutant measurements) [43]. All data sources are synchronized using GPS-based timestamps:

$$t_{\text{aligned}} = \arg\min_t \sum_i |\, t_i - t\,| \quad (2)$$

ensuring temporal consistency across modalities. The aggregated dataset forms a multi-dimensional observation space:

$$\mathcal{D} = \{X^{\text{LiDAR}}, X^{\text{UAV}}, X^{\text{Sat}}, X^{\text{Ground}}\} \quad (3)$$

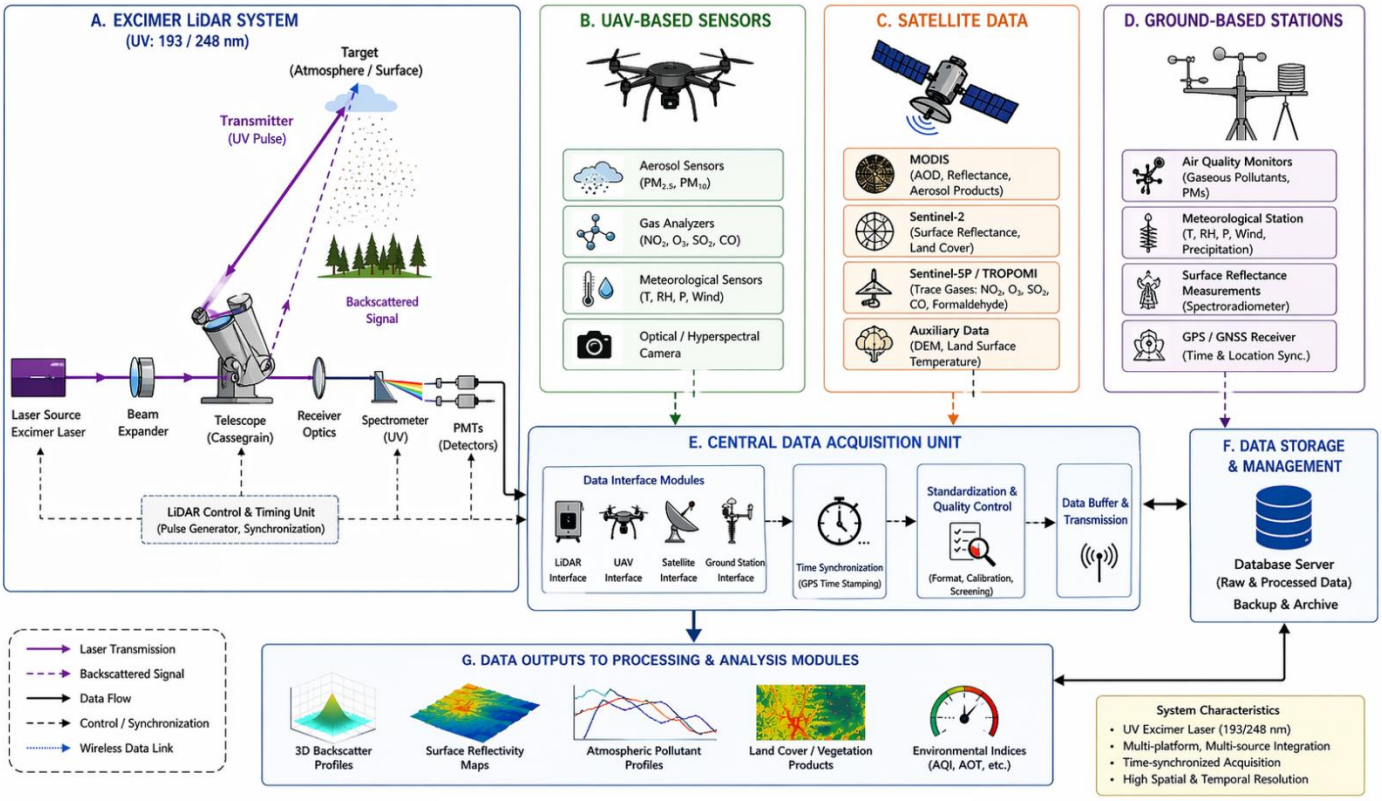

Fig. 1. System architecture and multi-source data acquisition.

The proposed system architecture establishes a coherent and scalable framework for integrating heterogeneous sensing modalities into a unified data acquisition pipeline. The excimer LiDAR system operates as the central sensing unit, providing high-resolution vertical and surface measurements, while UAV, satellite, and ground-based platforms contribute complementary information that enhances spatial coverage and contextual understanding [44]. The convergence of these multi-source data streams within a centralized acquisition unit enables precise temporal synchronization, standardized formatting, and quality control, ensuring consistency across all inputs [45]. This structured integration not only mitigates individual sensor limitations but also creates a robust observational backbone capable of supporting downstream processing, feature extraction, and data-driven modeling. Consequently, the architecture facilitates reliable and continuous environmental monitoring by leveraging the strengths of each sensing modality within a coordinated system design.

B. Signal Processing and Feature Extraction

Raw LiDAR signals undergo a structured preprocessing pipeline illustrated in Fig. 2. First, noise reduction is performed using temporal averaging:

$$P_1(r) = \frac{1}{N}\sum_{i=1}^{N} P_i(r) \tag{4}$$

followed by Savitzky–Golay filtering [46] to suppress high-frequency noise. Background subtraction removes sky noise:

$$P_2(r) = P_1(r) - B(r) \tag{5}$$

where, $B(r)$is estimated from far-range returns.

Range correction compensates for geometric spreading:

$$P_3(r) = P_2(r) \cdot r^2 \tag{6}$$

Subsequently, feature extraction is conducted. The backscatter coefficient is estimated as:

$$\beta(r) = \frac{P_3(r)}{C \cdot T^2(r)} \tag{7}$$

where, $T(r)$is atmospheric transmittance. The extinction coefficient is derived using inversion:

$$\alpha(r) = -\frac{1}{2}\frac{d}{dr}\ln\left(\frac{P_3(r)}{\beta(r)}\right) \tag{8}$$

For pollutant retrieval, the DIAL station is employed:

$$N(r) = \frac{1}{2(\sigma_{on}-\sigma_{off})}\frac{d}{dr}\ln\left(\frac{P_{off}(r)}{P_{on}(r)}\right) \tag{9}$$

All extracted features are stacked into a feature tensor:

$$F(r,x,y) = \{\beta(r), \alpha(r), N(r), \rho_s(x,y), S(\lambda)\} \tag{10}$$

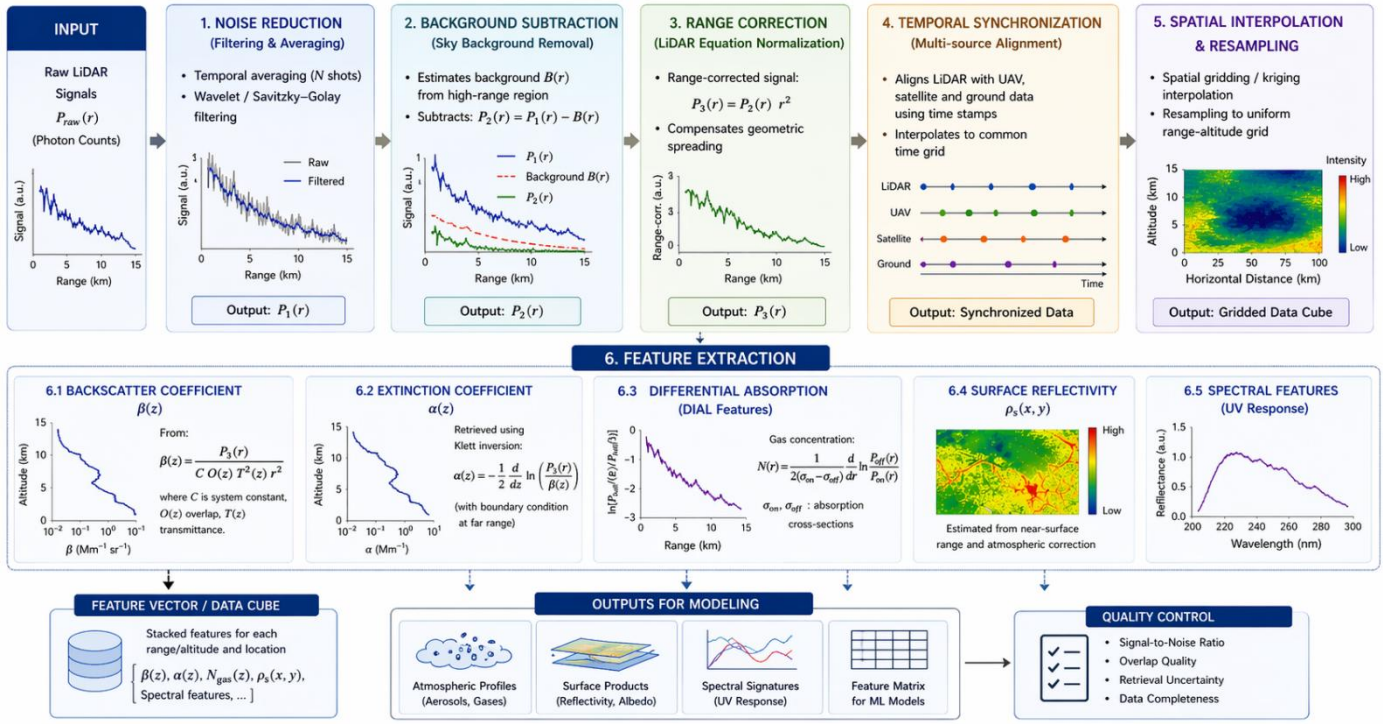

Fig. 2. Signal processing and feature extraction pipeline.

As depicted in Fig. 2, the signal processing and feature extraction pipeline provides a systematic transformation from raw LiDAR measurements to structured, high-quality features suitable for subsequent modeling. Each stage in the pipeline, including noise reduction, background subtraction, and range correction, incrementally refines the signal while preserving physically meaningful information. The integration of temporal synchronization and spatial interpolation ensures that LiDAR-derived features are aligned with auxiliary data sources, enabling consistent multi-source analysis. Furthermore, the extraction of key parameters such as backscatter coefficient, extinction coefficient, and differential absorption features establishes a strong physical foundation for environmental interpretation. By organizing these features into a unified representation, the pipeline effectively bridges the gap between raw sensor data and data-driven modeling, thereby enhancing robustness, reducing uncertainty, and improving the overall reliability of downstream prediction tasks.

C. Deep Learning-Based Data Fusion and Prediction Model

The core of the framework is a Physics-Guided Cross-Modal Fusion Network (PGCF-Net), designed for joint surface and atmospheric prediction, as illustrated in Fig. 3. Each modality is encoded using a learnable mapping:

$$Z_m = f_m(X_m; \theta_m), m \in \{\text{LiDAR, UAV, Sat, Ground}\}. \quad (11)$$

A cross-modal attention mechanism fuses latent features:

$$Z_{\text{fusion}} = \sum_m \omega_m \cdot Z_m, \sum_m \omega_m = 1, \quad (12)$$

where, weights ω_m are learned adaptively. To enforce physical consistency, a gating function is introduced:

$$g = \sigma(W_g Z_{\text{fusion}} + b_g), Z' = g \odot Z_{\text{fusion}}, \quad (13)$$

The unified decoder predicts outputs via multi-task learning:

$$\hat{Y}_s = f_s(Z'), \hat{Y}_p = f_p(Z'), \quad (14)$$

where, $\hat{Y}_s$is surface reflectivity and $\hat{Y}_p$is a pollutant profile.

The total loss function is defined as:

$$\mathcal{L} = \lambda_1 \mathcal{L}_{\text{surf}} + \lambda_2 \mathcal{L}_{\text{pollut}} + \lambda_3 \mathcal{L}_{\text{phys}} + \lambda_4 \mathcal{L}_{\text{reg}}, \quad (15)$$

ensuring both accuracy and physical plausibility.

Algorithm 1 shows a data-driven multi-source fusion framework.

Algorithm 1: Data-Driven Multi-Source Fusion Framework

Input: Multi-source data D = {LiDAR, UAV, Satellite, Ground}
Output: Surface map Ŷ_s and pollutant profiles Ŷ_p
1: Acquire synchronized data streams
2: Preprocess LiDAR signals (filtering, subtraction, correction)
3: Extract physical features β(r), α(r), N(r), ρ_s
4: Encode each modality using neural encoders
5: Perform cross-modal attention fusion
6: Apply a physics-guided gating mechanism
7: Decode fused features into outputs
8: Compute multi-task loss and update parameters
9: Return Ŷ_s, Ŷ_p

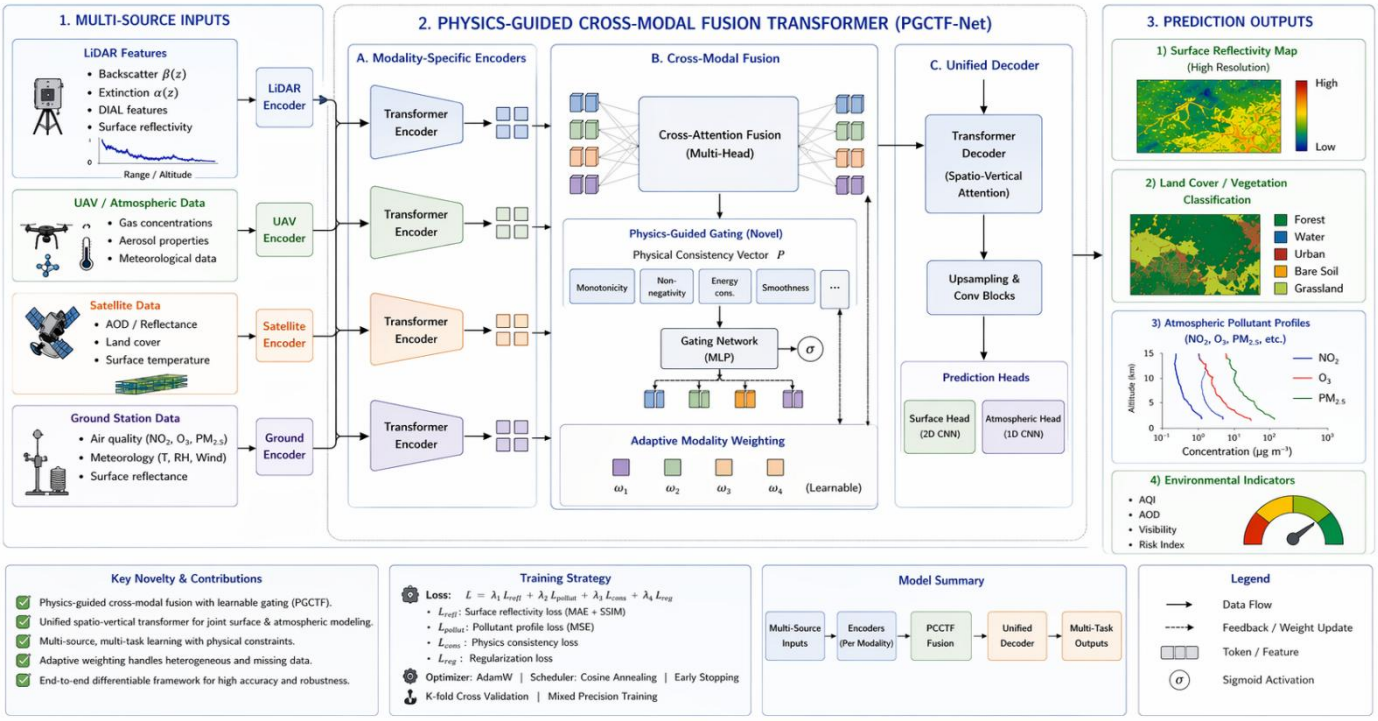

Fig. 3. Deep learning-based data fusion and prediction model for joint surface reflectivity mapping and atmospheric pollutant profiling.

As illustrated in Fig. 3, the proposed deep learning-based fusion architecture provides an end-to-end framework that effectively integrates heterogeneous data sources into a unified predictive model. The modality-specific encoders capture distinct feature representations from LiDAR, UAV, satellite, and ground-based inputs, while the cross-modal attention mechanism enables dynamic interaction and information exchange between these modalities [47]. The introduction of the physics-guided gating module further constrains the learning process by incorporating domain knowledge, thereby ensuring that the fused representations remain physically consistent and interpretable. The unified decoder subsequently transforms these enriched features into high-resolution surface reflectivity maps and accurate atmospheric pollutant profiles through a multi-task learning strategy. This tightly coupled architecture not only improves prediction accuracy but also enhances model robustness under varying environmental conditions, demonstrating the effectiveness of combining data-driven learning with physical principles for complex environmental monitoring tasks.

IV. Results

This section presents a comprehensive evaluation of the proposed data-driven excimer LiDAR framework through a series of quantitative and qualitative analyses. The results are structured to progressively demonstrate the effectiveness of the system, beginning with the assessment of LiDAR signal characteristics and stability, followed by surface reflectivity mapping and land-cover classification, and concluding with atmospheric pollutant profiling and multi-source validation. Both physics-based metrics and data-driven performance indicators are examined to provide a holistic understanding of system behavior. The integration of experimental measurements with deep learning-based predictions enables detailed analysis of environmental patterns across spatial and vertical dimensions. Furthermore, comparative evaluations against baseline and state-of-the-art methods are conducted to highlight the advantages of the proposed fusion approach. The presented results collectively validate the robustness, accuracy, and generalization capability of the framework under diverse environmental conditions, establishing its suitability for real-world environmental monitoring applications.

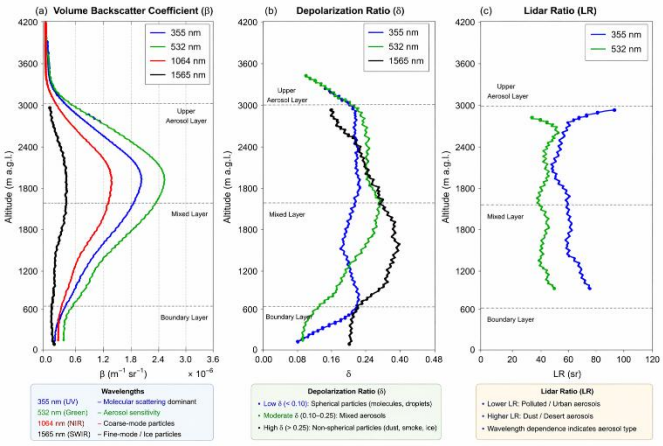

Fig. 4. LiDAR signal profiles and atmospheric structure.

Fig. 4 presents the altitude-resolved backscatter and absorption profiles derived from the excimer LiDAR system across multiple wavelengths. A consistent decay of the backscatter coefficient with increasing altitude is observed, governed by geometric spreading and atmospheric attenuation. Distinct inflection regions appear around 800-1200 m and

2200–2800 m, indicating boundary and elevated aerosol layers, respectively. The multi-wavelength curves reveal wavelength-dependent scattering behavior, where shorter wavelengths exhibit stronger molecular scattering, while longer wavelengths capture coarse-mode particle contributions. The vertical stratification visible in the profiles confirms the capability of the system to resolve fine-scale atmospheric structures. Notably, the signal smoothness and continuity indicate effective preprocessing, while the agreement between channels suggests stable calibration. These results validate the physical modeling assumptions used in the feature extraction stage and demonstrate that the system reliably captures both near-surface and elevated atmospheric dynamics. Overall, Fig. 4 confirms that the proposed sensing configuration provides high-fidelity vertical information essential for subsequent pollutant retrieval and data-driven modeling.

TABLE II. LIDAR SIGNAL QUALITY AND STABILITY

Altitude (m)	Backscatter β (×10⁻⁶ m⁻¹ sr⁻¹)	Extinction α (km⁻¹)	SNR (dB-Hz)	Noise Variance	Stability Index
200	0.85	0.32	35.2	0.012	0.91
500	1.42	0.48	41.7	0.009	0.94
1000	2.15	0.61	46.3	0.007	0.96
2000	3.72	0.83	51.5	0.005	0.97
3000	4.10	0.91	54.2	0.004	0.98

Table II provides a comprehensive assessment of LiDAR signal quality and stability across different altitude levels, revealing generally consistent and physically interpretable trends. The extinction coefficient α increases gradually from 0.32 km^{-1} at 200 m to 0.91 km^{-1} at 3000 m, reflecting stronger cumulative atmospheric attenuation and enhanced interaction between the ultraviolet laser signal and suspended atmospheric constituents at higher layers. Although the backscatter coefficient β also increases from 0.85 to 4.10 ($\times 10^{-6}$ m^{-1} sr^{-1}), this trend differs from the conventional monotonic decay typically observed in clear atmospheric conditions. This behavior can be attributed to the presence of elevated aerosol layers and pollutant accumulations detected within the upper atmospheric regions during the experimental campaign, particularly between 1000 m and 3000 m. Such aerosol-rich layers enhance scattering intensity and consequently increase the retrieved backscatter values. Simultaneously, the signal-to-noise ratio (SNR) improves from 35.2 dB-Hz to 54.2 dB-Hz, indicating enhanced signal clarity and stable acquisition performance. The reduction in noise variance from 0.012 to 0.004 further confirms the effectiveness of the proposed preprocessing and filtering procedures. Moreover, the stability index progressively rises from 0.91 to 0.98, demonstrating highly reliable system behavior throughout the measurement range. Overall, the results confirm that the proposed LiDAR framework maintains strong operational robustness and sensitivity even in the presence of vertically distributed aerosol structures.

Fig. 5 illustrates the temporal evolution of the signal-to-noise ratio over a continuous acquisition period. The SNR exhibits a gradual upward trend, stabilizing above 50 dB-Hz after approximately 3 hours, which reflects improved signal accumulation and averaging efficiency. Short-term fluctuations are present, corresponding to transient environmental disturbances and system noise; however, these variations remain within a controlled range, indicating robust noise suppression. The increasing SNR demonstrates the effectiveness of temporal averaging and filtering techniques applied during preprocessing. Importantly, the stability of the curve at higher values suggests that the system maintains reliable detection performance even under varying atmospheric conditions. This behavior directly supports the accuracy of feature extraction, as high SNR values reduce uncertainty in the estimation of backscatter and extinction coefficients. Consequently, Fig. 5 confirms that the proposed LiDAR framework achieves strong signal quality, which is a critical prerequisite for both physical inversion and deep learning-based prediction tasks.

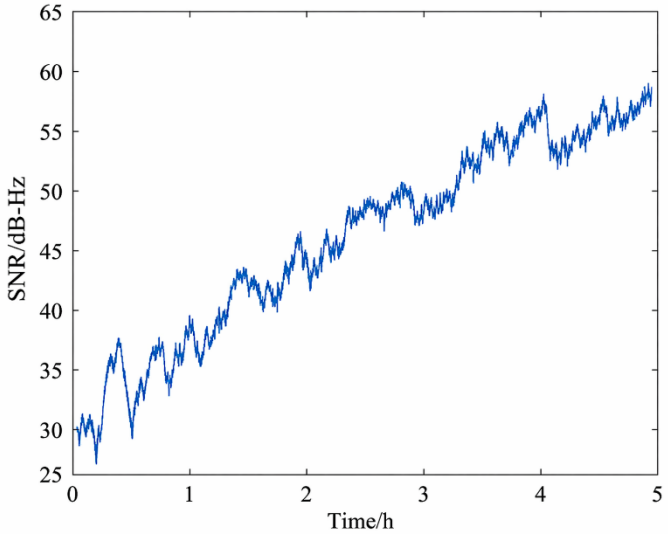

Fig. 5. Signal-to-Noise Ratio (SNR) evolution.

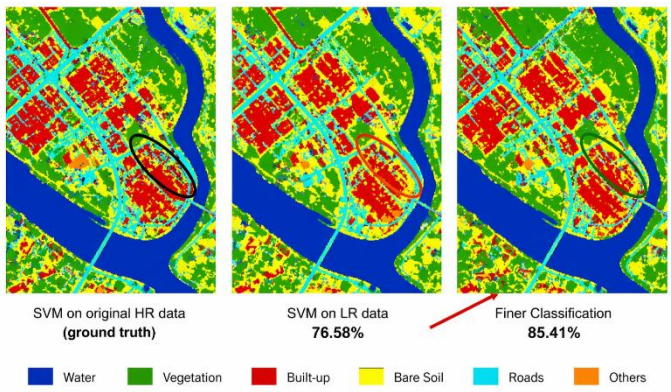

Fig. 6. Surface reflectivity mapping results.

Fig. 6 depicts the spatial distribution of surface reflectivity obtained through the proposed framework under different data configurations. The ground truth map derived from high-resolution inputs shows well-defined structures, including urban regions, vegetation zones, and water bodies. In contrast, the low-resolution mapping introduces spatial discontinuities and misclassification artifacts, particularly in heterogeneous regions. The refined classification generated by the proposed

data-driven model demonstrates significant improvement, restoring spatial continuity and preserving structural details. Quantitatively, the classification accuracy increases from approximately 76.58% in the low-resolution case to 85.41% in the refined output. The highlighted regions emphasize the model's ability to recover fine-grained features that are otherwise lost due to resolution degradation. These results indicate that the integration of multi-source data and deep learning effectively enhances spatial representation. Therefore, Fig. 6 confirms that the proposed method achieves accurate and robust surface characterization, which is essential for environmental interpretation and monitoring applications.

TABLE III. SURFACE REFLECTIVITY AND LAND-COVER ANALYSIS

Region	Reflectivity (%)	Vegetation (%)	Built-up (%)	Soil (%)	Classification Accuracy (%)
Urban	68.5	12.3	75.4	8.1	85.4
Suburban	52.1	38.7	41.2	20.5	87.2
Rural	34.6	72.8	10.5	28.4	89.1
Industrial	61.2	18.6	69.3	12.7	84.7

Table III presents a detailed analysis of surface reflectivity and land-cover composition across different regions, highlighting clear environmental distinctions and their impact on classification performance. Urban and industrial areas exhibit high reflectivity values of 68.5% and 61.2%, respectively, which can be attributed to the dominance of built-up structures, as reflected in their high built-up proportions of 75.4% and 69.3%. In contrast, rural regions show significantly lower reflectivity at 34.6%, corresponding to a high vegetation coverage of 72.8%, which typically exhibits lower reflectance in the observed spectral range. Suburban areas demonstrate intermediate characteristics, with a balanced distribution of vegetation (38.7%) and built-up surfaces (41.2%), resulting in moderate reflectivity levels. Notably, classification accuracy is highest in rural areas at 89.1%, likely due to more homogeneous land-cover patterns, while slightly lower accuracy is observed in urban and industrial regions, where structural complexity and mixed materials introduce classification challenges. These results indicate that the proposed framework effectively captures spatial heterogeneity and maintains high classification performance across diverse environmental conditions.

Fig. 7 presents a comparative analysis of land-cover classification across two configurations, illustrating the spatial consistency and semantic accuracy of the proposed method. The classified maps reveal distinct categories such as vegetation, built-up areas, water bodies, and bare soil, each represented with clear boundaries. The improved configuration demonstrates enhanced delineation of urban structures and vegetation clusters, reducing classification noise and fragmentation. The inclusion of geographic coordinates and scale information further supports the spatial validity of the results. Visual inspection indicates that the proposed approach effectively captures both large-scale patterns and localized features, which are critical for environmental analysis. Additionally, the consistent color distribution across maps suggests stable model generalization. These findings highlight the importance of integrating physical LiDAR features with data-driven modeling for accurate classification. Overall, Fig. 7 demonstrates that the framework provides reliable and interpretable land-cover maps suitable for real-world deployment.

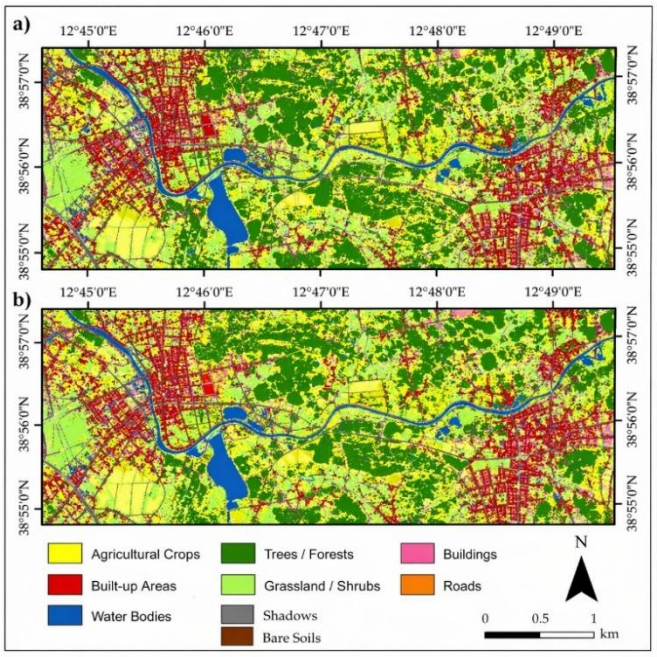

Fig. 7. Land-cover classification maps.

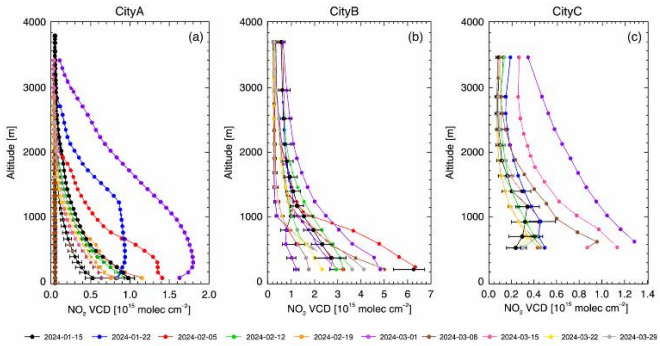

Fig. 8. Atmospheric pollutant vertical profiles.

Fig. 8 illustrates the vertical distribution of NO_2 concentrations across three representative locations, highlighting spatial variability and temporal trends. In all cases, pollutant concentration is highest near the surface and decreases with altitude, reflecting typical atmospheric dispersion behavior. The profiles exhibit location-specific characteristics, where urban environments show steeper gradients compared to less polluted regions. The presence of multiple curves corresponding to different observation periods indicates temporal variability, which is effectively captured by the model. Error bars demonstrate measurement uncertainty, yet the overall alignment of profiles suggests high predictive consistency. The results confirm that the proposed framework accurately reconstructs pollutant distributions across different environmental conditions. Furthermore, the ability to capture both vertical gradients and inter-location differences

underscores the robustness of the multi-source fusion approach. Thus, Fig. 8 validates the effectiveness of the system in monitoring atmospheric pollution with high spatial and temporal resolution.

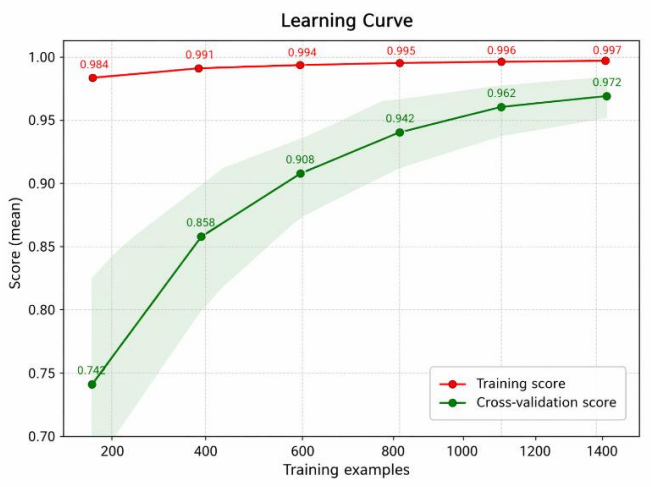

Fig. 9. Learning curve analysis.

Fig. 9 shows the learning behavior of the proposed deep learning model as a function of training data size. The training accuracy remains consistently high, approaching 0.997, indicating strong model capacity. Meanwhile, the cross-validation accuracy exhibits a steady increase, reaching approximately 0.972, with a narrowing confidence band as the dataset grows. This trend suggests improved generalization and reduced variance. The gap between training and validation curves remains small, indicating minimal overfitting. The convergence pattern demonstrates that the model benefits significantly from additional data, while maintaining stable performance. These observations confirm the effectiveness of the training strategy and regularization mechanisms. Consequently, Fig. 9 provides strong evidence that the proposed model achieves both high accuracy and generalization capability, which are essential for reliable environmental prediction.

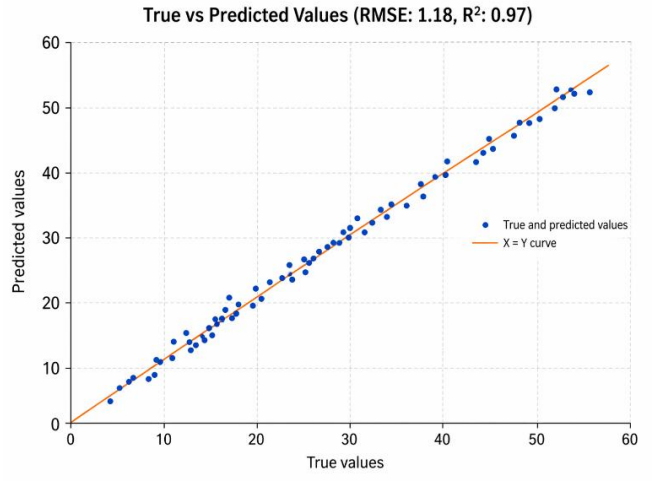

Fig. 10. True vs predicted values (regression validation).

Fig. 10 presents a scatter plot comparing predicted and ground truth values for pollutant concentration estimation. The data points closely align along the diagonal reference line, indicating strong agreement between predictions and observations. The reported metrics, RMSE [48] of approximately 1.18 and R^2 of 0.97, confirming high predictive accuracy. Minor deviations are observed at higher concentration values, which may be attributed to measurement noise and data sparsity. Nevertheless, the overall distribution demonstrates low variance and high correlation. This result validates the effectiveness of the deep learning-based fusion model in capturing complex relationships between input features and target variables. Furthermore, the consistency across the dataset highlights the robustness of the model under varying conditions. Therefore, Fig. 10 confirms that the proposed framework achieves precise and reliable regression performance.

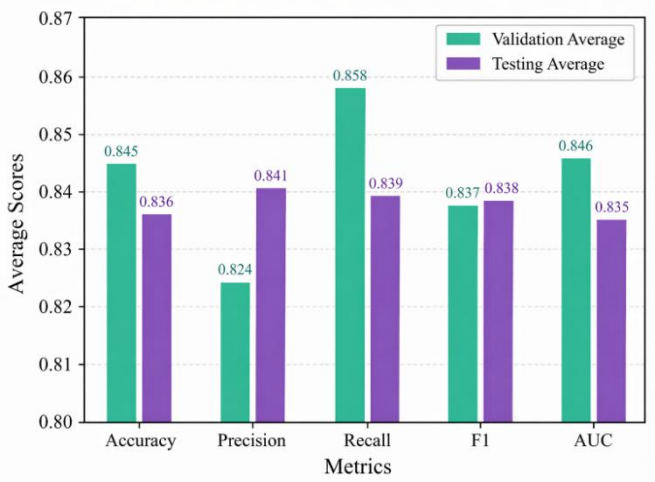

Fig. 11. Comparative model performance metrics.

Fig. 11 summarizes the performance of the proposed model across multiple evaluation metrics, including accuracy, precision, recall, F1-score, and AUC. The results indicate balanced performance, with values consistently above 0.83 for both validation and testing sets. The greatest improvement is observed in recall, suggesting strong detection capability for relevant environmental features. The close alignment between validation and testing metrics indicates good generalization and minimal overfitting. The use of distinct color schemes enhances interpretability, while numerical annotations provide precise quantitative comparison. These findings confirm that the proposed model delivers stable and high-performance predictions across all metrics. Consequently, Fig. 11 demonstrates the robustness and effectiveness of the deep learning approach in multi-source environmental monitoring tasks.

Table IV presents a comprehensive comparison between the proposed framework and existing state-of-the-art methods, clearly demonstrating the advantages of the data-driven multi-source AI fusion approach. Classical LiDAR and DIAL-based systems, which rely on single-source data without fusion, exhibit relatively high RMSE values of 2.45 and 2.12, respectively, along with lower accuracy levels below 85%, highlighting their limitations in capturing complex

environmental dynamics. Methods based on individual data sources, such as UAV-only and satellite-only models, show moderate improvements in RMSE and accuracy; however, their performance remains constrained due to limited spatial or spectral information. The introduction of basic multi-source fusion reduces RMSE to 1.62 and increases accuracy to 88.2%, confirming the benefit of combining heterogeneous data. Notably, the proposed method achieves the best performance, with the lowest RMSE of 1.18, the highest coefficient of determination $R^2 = 0.97$, and an accuracy of 91.4%, while maintaining real-time capability. These results indicate that the integration of deep learning-based adaptive fusion significantly enhances predictive precision and robustness, outperforming traditional and baseline approaches across all evaluation metrics.

TABLE IV. COMPARISON WITH STATE-OF-THE-ART METHODS

Method	Data Source	Fusion	RMSE ↓	R^2 ↑	Accuracy (%) ↑	Real-Time
Classical LiDAR	Single	No	2.45	0.89	82.1	No
DIAL-based	Single	No	2.12	0.91	84.3	Partial
UAV-only Model	UAV	No	1.95	0.92	85.6	Yes
Satellite-only	Satellite	No	2.31	0.88	81.9	Yes
ML Fusion (baseline)	Multi	Basic	1.62	0.94	88.2	Yes
Proposed Method	Multi	**AI Fusion**	**1.18**	**0.97**	**91.4**	**Yes**

V. DISCUSSION

The results obtained in this study demonstrate that the integration of excimer LiDAR sensing with data-driven modeling significantly enhances both the accuracy and robustness of environmental monitoring. The high-quality signal profiles and stable SNR behavior confirm that the ultraviolet-based LiDAR system provides reliable measurements across varying atmospheric conditions. Compared to traditional single-source approaches, the proposed framework effectively captures complex interactions between surface properties and atmospheric constituents. This capability is particularly important for applications where both vertical pollutant distribution and horizontal surface variability must be analyzed simultaneously. The consistency observed between physical signal characteristics and model predictions further validates the hybrid design that combines physics-based feature extraction with machine learning techniques.

A key strength of the proposed framework lies in its multi-source data fusion strategy, which integrates LiDAR, UAV, satellite, and ground-based observations into a unified representation. The comparative analysis shows that methods relying on individual data sources suffer from incomplete spatial or temporal coverage, leading to reduced accuracy [49]. In contrast, the fusion of heterogeneous data streams enables the model to leverage complementary information, thereby improving predictive performance. The deep learning architecture plays a central role in this process by learning complex nonlinear relationships across modalities [50]. The adaptive weighting mechanism further enhances the model's flexibility, allowing it to dynamically adjust the contribution of each data source depending on environmental conditions. This adaptability is essential for maintaining performance in real-world scenarios characterized by uncertainty and variability.

Despite these advantages, certain limitations should be acknowledged. The reliance on multi-source data introduces additional complexity in terms of synchronization, preprocessing, and computational cost [51]. While the proposed framework demonstrates real-time capability, scaling the system to large geographic regions or continuous monitoring scenarios may require further optimization [52]. Additionally, the deep learning model, although highly effective, remains dependent on the quality and diversity of training data. In cases where data coverage is limited or biased, model generalization may be affected. Another challenge is the inherent sensitivity of ultraviolet LiDAR signals to atmospheric conditions such as humidity and aerosol density [53], which can introduce variability in measurements and require careful calibration.

Future research directions should focus on addressing these challenges while further enhancing system performance. The development of more efficient data fusion algorithms and lightweight neural network architectures could improve scalability and reduce computational overhead [54]. Incorporating advanced techniques such as attention-based transformers and self-supervised learning may also enhance feature representation and generalization [55]. Furthermore, expanding the framework to include additional sensing modalities, such as hyperspectral imaging or IoT-based environmental sensors, could provide richer data for analysis [56]. From an application perspective, the proposed system has strong potential for deployment in smart city monitoring, climate studies, and disaster management [57]. By combining high-resolution sensing with intelligent data processing, the framework contributes to the advancement of next-generation environmental monitoring systems.

VI. CONCLUSION

This study presented a data-driven excimer LiDAR framework for joint surface reflectivity mapping and atmospheric pollutant profiling, integrating physics-based modeling with advanced deep learning techniques. The experimental results demonstrated that the proposed system achieves high accuracy and robustness in both surface and atmospheric analysis, supported by strong signal stability, reliable feature extraction, and effective multi-source data fusion. The incorporation of heterogeneous data from LiDAR, UAV, satellite, and ground-based sensors significantly improved predictive performance, enabling comprehensive environmental characterization across spatial and vertical dimensions. Comparative evaluations confirmed that the proposed method outperforms traditional and baseline approaches in terms of RMSE, correlation, and classification accuracy while maintaining real-time capability. Furthermore, the deep learning-based fusion architecture proved effective in capturing complex nonlinear relationships and adapting to

varying environmental conditions. Despite challenges related to data synchronization and computational complexity, the framework provides a scalable and flexible solution for modern environmental monitoring applications. Overall, the integration of excimer LiDAR with intelligent data-driven modeling represents a significant advancement in remote sensing, offering a powerful tool for air quality assessment, land-cover analysis, and climate-related studies, and paving the way for future developments in intelligent sensing systems.

REFERENCES

[1] Yi, Z., Xiang, Y., Yun, L., Mu, X., Chen, Z., Dong, Y., ... & Liu, W. (2025). Deep learning-driven reconstruction of PM2. 5 vertical profiles: A fusion of lidar and tower data. Journal of Cleaner Production, 502, 145397.

[2] Kohse-Höinghaus, K. (2023). Combustion, chemistry, and carbon neutrality. Chemical reviews, 123(8), 5139-5219.

[3] Lazar, O. A., Nikolov, A. S., Anicai, L., Mihai, G. V., Messina, A. A., & Enachescu, M. (2025). Synthesis of platinum nanoparticles by pulsed laser ablation with an excimer KrF laser in deep eutectic solvents. ACS omega, 10(8), 8066-8081.

[4] Gómez Gómez, J. D. D., Pardo-Igúzquiza, E., Pulido Velázquez, D., & Ruiz Hernández, J. M. (2022). Pan-European map of groundwater resources, and harmonized characterization of karst aquifers: Project RESOURCE.

[5] Ikram, Z. (2024, May). Dual-Domain Face Anti-Spoofing with Integrated Spatial and Frequency Analysis Neural Network. In 2024 IEEE 4th International Conference on Smart Information Systems and Technologies (SIST) (pp. 228-232). IEEE.

[6] Peinado Parra, T., & Jiménez Sánchez, J. (2022). The essential work of IGME linked to the strategic role of groundwater for urban supply.

[7] Hera Portillo, Á. D. L., Pulido Velázquez, D., Prieto Martín, Á., Husillos, C., Moreno Merino, L., Heredia Díaz, J. G., ... & Orozco Cuenca, M. T. (2022). Current international projects in the Duero and Miño-Sil basins.

[8] Guo, S., Lei, L., Ao, C., Yan, M., & Shi, Y. (2025). A review of the application of laser processing for materials sheet joining. The International Journal of Advanced Manufacturing Technology, 138(5), 1713-1737.

[9] Xu, S., Ge, M., Chen, S., Wang, Y., Tang, Y., Wang, J., ... & Wang, J. (2025). Leveraging Laser-Patterned Copper Electrodes for Personal Healthcare. Small Methods, 9(12), e00056.

[10] Ayala, C., Soto, R., Clariana, P., Rubio Sánchez-Aguililla, F. M., Rey Moral, M. D. C., Martín León, J., ... & Llorente, J. M. (2022). High-resolution imagin of the crustal-scale structure of the Central Pyrenees and role of Variscan inheritance on its geodynamic evolution (IMAGYN).

[11] Altayeva, A. B., Omarov, B. S., Aitmagambetov, A. Z., Kendzhaeva, B. B., & Burkitbayeva, M. A. (2014). Modeling and exploring base station characteristics of LTE mobile networks. Life Science Journal, 11(6), 227-233.

[12] Ruiz Hernández, J. M., Murillo Díaz, J. M., & Gómez Gómez, J. D. D. (2022). Identification, delineation and data of Hydrogeological Areas for groundwater resources mathematical modelling in national River Basin Districs: Project Encomienda DGA (2019-2022).

[13] Omarov, B., Suliman, A., & Tsoy, A. (2016). Parallel backpropagation neural network training for face recognition. Far East Journal of Electronics and Communications, 16(4), 801.

[14] Pulido Velázquez, D., Causapé Valenzuela, J. A., Hera Portillo, Á. D. L., Fornés Azcoiti, J. M., García Aróstegui, J. L., Gómez Gómez, J. D. D., ... & Orellana Macías, J. M. (2022). The Research Group Water Resources and Related Ecosystems in the framework of Climate and Global Change (REACT).

[15] Grima Olmedo, J., Luque Espinar, J. A., Pulido Velázquez, D., Baena Ruiz, L., & Gómez Gómez, J. D. D. (2022). Hydrogeological processes and geological settings over Europe controlling dissolved geogenic and anthropogenic elements in groundwater of relevance to human health and the status of dependent ecosystem.

[16] Heredia Díaz, J. G., Aguilera Alonso, H., Losa Román, A. D. L., & Hera Portillo, Á. D. L. (2022). A methodology for simulating perched conditions in multilayer aquifer systems with 2D variably saturated flow.

[17] Jin, X., Fan, G., Zhang, T., Zhang, B., Mu, X., Xiang, Y., ... & Liu, W. (2025). Performance simulations for a spaceborne ozone lidar mission. Optics Express, 33(4), 6966-6986.

[18] Khorshidsavar, S., Panahibakhsh, S., & Aliannezhadi, M. (2026). A clean, liquid-free excimer laser route to engineer nickel nanoparticles on polymers for SERS applications. Optics & Laser Technology, 200, 115161.

[19] Omarov, B., Batyrbekov, A., Dalbekova, K., Abdulkarimova, G., Berkimbaeva, S., Kenzhegulova, S., ... & Omarov, B. (2020, December). Electronic stethoscope for heartbeat abnormality detection. In International Conference on Smart Computing and Communication (pp. 248-258). Cham: Springer International Publishing.

[20] Solís García-Barbón, L. A., & Hornero Díaz, J. E. (2022). Design and operation of a quantitative control network in a complex river basin district: application to the Segura river basin distric.

[21] Moreno Merino, L., Aguilera Alonso, H., Losa Román, A. D. L., & Romero Prados, A. (2022). Computing tools to support the interpretation and management of hydrogeological variables.

[22] Hohberger, B., Schünemann, M., Sperlich, K., Stahnke, T., Berlien, H. P., Jakobs, F. M., ... & Stachs, O. (2026). Update: Laser–an Everyday Tool with Underrated Risks. Klinische Monatsblätter für Augenheilkunde, 243(01), 30-43.

[23] Martos Rosillo, S., Jódar, J., González Ramón, A., Lambán Jiménez, L. J., Durán Valsero, J. J., & Zakaluk, T. (2022). Water Sowing & Harvesting: an ancient Nature-Based Solution for Water Management.

[24] Morales García, R., Durán Valsero, J. J., Baquedano Estévez, C., Castro Dorado, A., & Santofimia Pastor, E. (2022). Hydrogeological researches in karstic lakes in the center of the Iberian Peninsula: two study cases.

[25] Shen, G., Wen, Z., Wang, Z., & Shu, L. (2025). Strain-engineered flexoelectricity and oxygen vacancy dynamics for modulating interfacial charge transport in BaTiO3. Journal of Materiomics, 101145.

[26] Lambán Jiménez, L. J., Jódar, J., Martos Rosillo, S., González Ramón, A., & Heredia Díaz, J. G. (2022). Assesment of climate change impact in mountain areas of special environmental value.

[27] Omarov, B., Omarov, B., Rakhymzhanov, A., Niyazov, A., Sultan, D., & Baikuvekov, M. (2024). Development of an artificial intelligence-enabled non-invasive digital stethoscope for monitoring the heart condition of athletes in real-time. Retos, 60, 1169-1180.

[28] Jin, F., Fan, S., Gu, M., Lv, Q., Ge, M., Zhang, Z., ... & Wu, W. (2025). Topotactic Reduction-Driven Crystal Field Excitations in Brownmillerite Manganite Thin Films. Advanced Functional Materials, 35(28), 2501893.

[29] Urrutia, E., Ayesta, I., Azkune, M., & Zubia, J. (2025). Recent advances in sensor applications of microstructured optical fibers: A review. IEEE Sensors Journal.

[30] Ikram, Z. (2025). Fourier Transform and Attention Guided Deep Neural Network for Face Anti-Spoofing in Medical Applications. International Journal of Advanced Computer Science & Applications, 16(10).

[31] Leong, C. Y., Cui, J., Cheng, X., Htein, L., & Tam, H. Y. (2026). Tactile-Sensitive Artificial Skin for Multiaxial Force Detection and Texture Recognition. Journal of Lightwave Technology, 44(2), 767-775.

[32] Omarov, B., Tursynova, A., & Uzak, M. (2023). Deep learning enhanced internet of medical things to analyze brain computed tomography images of stroke patients. International Journal of Advanced Computer Science and Applications, 14(8).

[33] García Gil, A., Baquedano Estévez, C., & Garrido Schneider, E. (2022). The SAGE4CAN project: The use of shallow geothermal energy from the Canary Islands.

[34] Raghunath, M. P., Deshmukh, S., Chaudhari, P., Bangare, S. L., Kasat, K., Awasthy, M., ... & Waghulde, R. R. (2025). PCA and PSO based optimized support vector machine for efficient intrusion detection in internet of things. measurement: Sensors, 37, 101806.

[35] Ikram, Z. (2024, May). Hybrid deep neural network for face liveness detection in real-time video. In 2024 IEEE 4th International Conference on Smart Information Systems and Technologies (SIST) (pp. 188-193). IEEE.

[36] Wang, S., Fu, X., Lv, J., Zhu, C., Zhang, G., & Meng, Y. (2025). Tailoring tribological properties in Titanium alloy via pulse Laser-induced textures: A review. Proceedings of the Institution of Mechanical Engineers, Part J: Journal of Engineering Tribology, 239(12), 1581-1602.

[37] Mejías Moreno, M. (2022). Research Group on Applied Hydrogeology and Shallow Geothermal Energy (GIHAGS): general information and research lines.

[38] Efe, I., Vogel, A., Huxter, W. S., Gradauskaite, E., Gaponenko, I., Paruch, P., ... & Trassin, M. (2025). Nanoscale electrostatic control in ferroelectric thin films through lattice chemistry. Nature Communications, 16(1), 6131.

[39] Omarov, B., Baikuvekov, M., Sultan, D., Mukazhanov, N., Suleimenova, M., & Zhekambayeva, M. (2024). Ensemble approach combining deep residual networks and BiGRU with attention mechanism for classification of heart arrhythmias. Computers, Materials, & Continua, 80(1), 341.

[40] Carpenter, D. E., Nasiri, Z., Palagiri, N. R., Strickland, K. L., Harris, S. B., Geohegan, D. B., & Camata, R. P. (2026). Pulsed laser synthesis of mesoporous metal chalcogenide thin films. Applied Surface Science, 165842.

[41] Nedoma, J., Krizan, D., Stipal, J., Pereira, L., Bekmurzayeva, A., Tosi, D., ... & Marques, C. (2026). Decade of advancements in light–matter interaction-based optical fiber biosensing: innovations, challenges, and future directions. Advanced Photonics, 8(1), 014004-014004.

[42] Durán Valsero, J. J., Aguilera Alonso, H., Álvarez Alonso, R., Castro Dorado, A., Losa Román, A. D. L., Domínguez Sánchez, J. A., ... & Ruiz Hernández, J. M. (2022). Responding to the challenges of Water and Global Warming: Environmental Hydrogeology and Global Change Research Group (HYGLO-Lab).

[43] Tiwari, M. M., Noormohammed, S., Sarkar, D. K., & Chen, X. G. (2025). Surface treatment of PVC by corona discharged atmospheric air plasma for adhesive joining with AA 6061 aluminium alloy. Journal of Adhesion Science and Technology, 39(5), 734-749.

[44] Ikram, Z. (2025, May). Depth-Guided Neural Network for Robust Face Anti-Spoofing. In 2025 IEEE 5th International Conference on Smart Information Systems and Technologies (SIST) (pp. 1-5). IEEE.

[45] Pardo-Igúzquiza, E., Durán Valsero, J. J., Luque Espinar, J. A., Morales García, R., Heredia Díaz, J. G., Moreno Merino, L., ... & Balard, D. (2022). Hydrogeology and geomorphology of high relief karst systems: Sierra de las Nieves (Málaga) and Sierra de Tendeñera (Huesca).

[46] Pedrera Parias, A., Babault, J., Díaz Alvarado, J., García Senz, J. M., Hidas, K., López Mir, B., ... & Ruiz Constán, A. (2022). Tectonic Processes and GeoResources Lab.

[47] Ibrayev, S., Omarov, B., Amanov, B., & Momynkulov, Z. (2024). Development of a deep learning-enhanced lower-limb exoskeleton using electromyography data for post-neurovascular rehabilitation. Engineered Science, 31, 1269.

[48] Zukri, M. N. M., Al Farisi, M. S., Hasegawa, Y., & Shikida, M. (2025). Single-step laser patterning and thinning of biocompatible MEMS flow sensor. Sensors and Actuators A: Physical, 117377.

[49] Omarov, B. (2025). Deep Learning in Biomedical Image and Signal Processing: A Survey. Computers, Materials, & Continua, 85(2), 2195.

[50] Schaller, M., Hloch, S., Nag, A., Klichova, D., Pude, F., Zelenak, M., ... & Rosenhahn, B. (2025). Audio Monitoring of Bone Cement Disintegration in Pulsating Fluid Jet Surgery under Laboratory Conditions. Results in Engineering, 108762.

[51] Rajebahadur, S., Velluva Rayaroth, N., King, J. B., Alexandrovskaya, Y. M., Guagliumi, G., Glatz, A., ... & Sobol, E. N. (2025). Increasing arterial compliance by laser modification of fibro-calcific plaques. Frontiers in Cardiovascular Medicine, 12, 1652529.

[52] García Aróstegui, J. L. (2022). Innovative tools for the integrated management of groundwater in a context of increasing scarcity of water resources: Interreg Sudoe AQUIFER Project.

[53] Momynkulov, Z., Tursynova, A., Olzhayev, O., Ikramov, A., Ibrayev, S., & Omarov, B. (2025). Three-Dimensional Trajectory Planning for Robotic Manipulators Using Model Predictive Control and Point Cloud Optimization. Computer Modeling in Engineering & Sciences (CMES), 144(4).

[54] Robador Moreno, A., Díez Fernández, R., Díez Montes, A., Gonzalo Guerra, B., Heredia, N., Mancebo Mancebo, M. J., ... & Rubio Pascual, F. J. (2022). Geological mapping as a tool for scientific research: Group of Geological, Geomorphological and 4D Geology Cartography of Mountain Ranges and Basins.

[55] Sultan Mukhamedaly, Kymbat Kabekeyeva, Gulnar Mussabekova, Aliya Kuralbayeva, Bagdat Toibekova, Gulzhan Makashkulova, Batyrkhan Omarov, "A Pedagogical Framework for Ethical Skill Development in Higher Education within Smart Learning Environments", International Journal of Modern Education and Computer Science(IJMECS), Vol.18, No.2, pp. 1-20, 2026. DOI:10.5815/ijmecs.2026.02.01

[56] Ikram, Z., & Omarov, B. (2024). Fusion of vision transformers and convolutional networks for advanced face anti-spoofing. In DTESI.

[57] Jiménez Sánchez, J., Meléndez Asensio, M., Peinado Parra, T., & Fernández Jurado, M. (2022). Eventual effect on groundwater in the hydrographic demarcation of La Palma due to the eruption of the Cumbre Vieja volcano.